The Reaction of Dimethyl Ether with Hydroxyl Radicals - Kinetic Isotope Effect and Pre-reactive Complex Formation.

ARTICLE *in* THE JOURNAL OF PHYSICAL CHEMISTRY A · AUGUST 2013

Impact Factor: 2.69 · DOI: 10.1021/jp405724a · Source: PubMed

4 AUTHORS, INCLUDING:

Johannes Kiecherer
Karlsruhe Institute of Technology
3 PUBLICATIONS **10** CITATIONS

SEE PROFILE

Milán Szőri
University of Szeged
41 PUBLICATIONS **338** CITATIONS

SEE PROFILE

THE JOURNAL OF PHYSICAL CHEMISTRY A

Article

pubs.acs.org/JPCA

Reaction of Dimethyl Ether with Hydroxyl Radicals: Kinetic Isotope Effect and Prereactive Complex Formation

Cornelie Bänsch, Johannes Kiecherer, Milan Szöri,[†] and Matthias Olzmann*

Institut für Physikalische Chemie, Karlsruher Institut für Technologie (KIT), Kaiserstr. 12, 76131 Karlsruhe, Germany

Supporting Information

ABSTRACT: The kinetic isotope effect of the reactions OH + CH_3OCH_3 (DME) and OH + CD_3OCD_3 (DME-d_6) was experimentally and theoretically studied. Experiments were carried out in a slow-flow reactor at pressures between 5 and 21 bar (helium as bath gas) with production of OH by laser flash photolysis of HNO_3 and time-resolved detection of OH by laser-induced fluorescence. The temperature dependences of the rate coefficients obtained can be described by the following modified Arrhenius expressions: $k_{OH+DME} = (4.5 \pm 1.3) \times 10^{-16}\ (T/K)^{1.48}\ \exp(66.6\ K/T)\ cm^3\ s^{-1}$ (T = 292−650 K, P = 5.9−20.9 bar) and $k_{OH+DME\text{-}d6} = (7.3 \pm 2.2) \times 10^{-23}\ (T/K)^{3.57}\ \exp(759.8\ K/T)\ cm^3\ s^{-1}$ (T = 387−554 K, P = 13.0−20.4 bar). A pressure dependence of the rate coefficients was not observed. The agreement of our experimental results for k_{OH+DME} with values from other authors is very good, and from a fit to all available literature data, we derived the following modified Arrhenius expression, which reproduces the values obtained in the temperature range T = 230−1500 K at pressures between 30 mbar and 21 bar to better than within ±20%: $k_{OH+DME} = 8.45 \times 10^{-18}\ (T/K)^{2.07}\ \exp(262.2\ K/T)\ cm^3\ s^{-1}$. For $k_{OH+DME\text{-}d6}$, to the best of our knowledge, this is the first experimental study. For the analysis of the reaction pathway and the kinetic isotope effect, potential energy diagrams were calculated by using three different quantum chemical methods: (**I**) CCSD(T)/cc-pV(T,Q)Z//MP2/6-311G(d,p), (**II**) CCSD(T)/cc-pV(T,Q)Z//CCSD/cc-pVDZ, and (**III**) CBS-QB3. In all three cases, the reaction is predicted to proceed via a prereaction OH−ether complex with subsequent intramolecular hydrogen abstraction and dissociation to give the methoxymethyl radical and water. Overall rate coefficients were calculated by assuming a thermal equilibrium between the reactants and the prereaction complex and by calculating the rate coefficients of the hydrogen abstraction step from canonical transition state theory. The results based on the molecular data from methods (**I**) and (**II**) showed a satisfactory agreement with the experimental values, which indicates that the pre-equilibrium assumption is reasonable under our conditions. In the case of method (**III**), the isotope effect was significantly underpredicted. The reason for this discrepancy was identified in a fundamentally differing reaction coordinate. Obviously, the B3LYP functional applied in method (**III**) for geometry and frequency calculations is inadequate to describe such systems, which is in line with earlier findings of other authors.

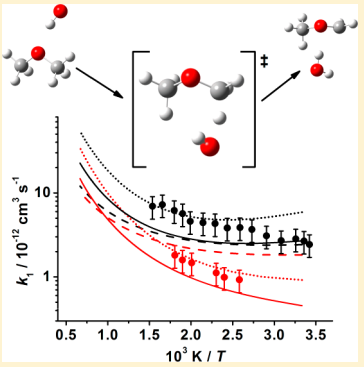

1. INTRODUCTION

Ethers are solvents widely used in laboratory and industry due to their excellent solvating properties and chemical inertness. In view of their low ignition temperatures, the understanding of the ignition processes for instance on hot surfaces is of relevance for occupational safety. Ethers are also discussed as alternative biofuels or fuel additives.[1] In particular, dimethyl ether (DME), with its high cetane number and favorable carbon/oxygen ratio, is currently explored as an alternative diesel fuel.[2] For a detailed understanding of desirable and undesirable ignition of ethers, reliable kinetic parametrizations of the ignition/oxidation mechanisms are required. In these mechanisms, the H abstraction by OH radicals is one of the most important steps. For the corresponding reaction of DME

$$CH_3OCH_3 + OH \rightarrow CH_3OCH_2 + H_2O \qquad (R1)$$

a considerable number of experimental[3−14] and theoretical[15−21] studies on the kinetics have already been published. In the experiments, several different time-resolved detection techniques for OH were used such as laser-induced fluorescence (LIF),[3−7] resonance absorption,[8,9] or resonance fluorescence,[10,11] and also a number of relative rate studies were performed.[9,12−14] These studies spanned a temperature range from 230 to 1500 K at pressures between 0.03 and 3 bar. It turned out that the temperature dependence of the rate coefficients from the different authors is essentially consistent and that there is no noticeable pressure dependence.[8]

From the theoretical studies, it follows that two types of hydrogen atoms in DME have to be distinguished,[15−19] which are usually denoted by in plane (ip) and out of plane (op).

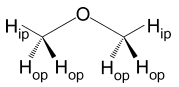

Consequently, the overall abstraction reaction R1 can proceed via two different types of transition states, TS(ip)

Received: June 10, 2013
Revised: August 5, 2013
Published: August 5, 2013

and TS(op), respectively. Regarding the detailed mechanism, most of the recent quantum chemical investigations[17−20] indicate the formation of weakly bound complexes in the entrance and exit channels. Accordingly, reaction R1 is likely to proceed via three consecutive steps. At first, a prereaction complex (reactant complex, RC) is formed, in which the H atom of the OH radical is weakly bonded to the O atom of the ether

$$(CH_3)_2O + OH \rightleftharpoons (CH_3)_2O\cdots HO \quad \text{(R1a)}$$

In the second, unimolecular step, an H atom from a methyl group is abstracted, and a postreaction complex (product complex, PC) between the methoxymethyl radical (dimethyl ether radical, DMER) and water is formed

$$(CH_3)_2O\cdots HO \rightarrow CH_3(CH_2)O\cdots HOH \quad \text{(R1b)}$$

Because of the exoergicity of reaction R1b, this complex rapidly decomposes to give the end products

$$CH_3(CH_2)O\cdots HOH \rightarrow CH_3OCH_2 + H_2O \quad \text{(R1c)}$$

Accordingly, reaction R1c is not rate-limiting, so reaction R1b is effectively irreversible.

Most quantum chemical calculations predict a lower energy for TS(op) than for TS(ip),[15,17−20] but in some cases, only TS(op) is correlated to the prereaction complex, whereas TS(ip) is directly correlated to the reactants.[17,19,20] In general, density functional theory (DFT) proves problematic for this reaction system. A large number of functionals has been tested but inconsistent results were obtained.[16−18] In particular, the prereaction complex is often not found,[16] which might be due to the fact that current density functionals (based on local density, its gradient, and the local kinetic-energy density) have limitations in the description of the (nonlocal) dispersion energy in noncovalent complexes.[22]

Rate coefficients of reaction R1 were calculated from quantum chemical data by using different kinds of transition state theory with tunneling corrections.[15,17−20] A very good agreement with experimental results over a large range of temperatures was achieved in a recent work by Zhou et al.,[19] where rate coefficients were obtained from variational RRKM theory with molecular data from quantum chemical calculations at CCSD(T)/CBS//MP2/6-311G(d,p) and G3 level of theory.

The use of canonical transition state theory for reactions via prereaction complexes requires the establishment of equilibrium between the bimolecular reactants and the prereaction complexes. This requirement is better fulfilled at higher pressures. Reaction R1 so far was experimentally studied at pressures up to 3 bar. In this work, we report on experiments in the pressure range 5−21 bar to further verify the equilibrium assumption. We analyze our results, using canonical transition state theory with molecular and transitions state data from high-level quantum chemical calculations. To get additional information and a more consistent data set, we also study the isotope effect[23] on reaction R1. Because to the best of our knowledge, rate coefficients of the DME-d_6 + OH reaction have not yet been measured, we also perform experiments on this reaction. In this way, an additional verification of the general mechanism and the quality of the quantum chemical results can be achieved.

2. EXPERIMENTAL SECTION

The experiments were performed in a slow-flow reactor with helium as the bath gas by using pulsed laser photolysis/laser-induced fluorescence for production/detection of OH radicals in an excess of DME to ensure pseudofirst-order conditions. The experimental setup was already described in detail elsewhere,[24−27] and hence, only a short summary is given here. The reactor is a T-shaped stainless steel cell equipped with three quartz windows and surrounded by resistance heating wires. The temperature was measured at the entrance and exit of the cell with thermocouples, and the difference between the two values never exceeded 10 K. The average was taken as reaction temperature. The gas flow was controlled by a mass flow controller, and accumulation of reaction products was avoided by choosing appropriate flow velocities.

Nitric acid was used as a precursor for the OH radicals. It was photolyzed with a KrF-excimer laser at a wavelength of 248 nm. The probe laser system consisted of a dye laser operated with Coumarin 153 and pumped by a XeCl-excimer laser at 308 nm. The frequency of the dye laser output was doubled with a BBO crystal to obtain the OH excitation wavelength of 281.9 nm. The nonresonant fluorescence of OH at 308 ± 7.5 nm was detected perpendicular to the antiparallel photolysis and probe laser beam. The influence of scattered light was minimized by filtering out other wavelengths with a monochromator. The temporal resolution of the experiment was achieved by changing the time delay between the photolysis and probe laser pulses in steps of 0.2 μs with a delay generator. For each given delay time, ten measurements were recorded and automatically averaged. The repetition rate was 5 Hz. More details of our approach can be found in ref 28 and the literature cited therein.

The gas mixtures were prepared manometrically in gas cylinders and stored for at least 12 h before use. The measured rate coefficients did not show any systematic dependence on the cylinder filling level, which indicates a complete homogenization of the gas mixtures. Because of the multitude of factors (temperature, pressure, initial concentrations of different mixtures prepared at different pressures, laser intensities, etc.), which influence the uncertainty of the experiments and are difficult to quantify exactly, a maximum error of 30% for the rate coefficients was estimated. We note, however, that the statistical error of one experimental run is usually much smaller (see below).

Nitric acid was freshly prepared and stored in the dark. For the synthesis, concentrated sulfuric acid was degassed and added to dried sodium nitrate. This reaction mixture was slowly heated up to 333 K, and in a direct vacuum distillation, nitric acid was collected in a separate flask cooled with liquid nitrogen; it was degassed before use. The purities of the other substances were as follows: He > 99.999% (Air Liquide), DME > 99% (Sigma-Aldrich), DME-d_6 > 99% (Sigma-Aldrich). The isotopic purity of DME and DME-d_6 was verified by mass spectrometry.

3. COMPUTATIONAL SECTION

3.1. Structures and Energies. Geometries and frequencies of the stationary points along the reaction pathway DME + OH → DMER + H_2O were calculated by using both second-order Møller−Plesset perturbation theory (MP2)[29,30] with the Gaussian split valence basis set 6-311G(d,p)[30,31] and coupled cluster theory with single and double excitations (CCSD)[32,33]

dx.doi.org/10.1021/jp405724a | J. Phys. Chem. A 2013, 117, 8343−8351

employing Dunning's correlation-consistent polarized valence double-ζ (cc-pVDZ)[34,35] basis set. Additionally, single-point calculations at the CCSD(T) level of theory (that is, including a perturbative treatment of triple excitations)[36] were performed for energies of the minimum structures and transition states with several correlation-consistent cc-pVXZ (X = D, T, and Q)[34,35] basis sets to extrapolate to the complete basis set (CBS) limit. Here, the Hartree−Fock and the correlation energy were treated separately. For the Hartree−Fock energy, we used $E_{HF}(X) = E^{\infty}_{HF} + b\exp(-cX)$ with $X = 2$, 3, and 4 for cc-pVDZ, cc-pVTZ, and cc-pVQZ, respectively;[37] for the correlation energy, we used $E_{corr}(X) = E^{\infty}_{corr} + b'X^{-3}$ with $X = 3$ and 4 for cc-pVTZ and cc-pVQZ, respectively.[38] To assess possible multireference character of the wave functions, T_1 diagnostics[39] were computed. The analysis showed that single-reference methods provide an adequate description in most cases. The largest T_1 diagnostics value is 0.02 for the TS(op) structure calculated at CCSD/cc-pVDZ level of theory, which is at the onset of important nondynamical correlation effects as suggested by Lee and Taylor.[39]

To gain information about the suitability of DFT[40] and in particular on the B3LYP[41,42] functional for the description of the DME + OH reaction, we also applied the CBS-QB3 method,[43] in which DFT at the B3LYP/6-311G(2d,d,p) level is applied for the calculation of geometries and frequencies. To characterize the minimum energy path on the potential energy surface, intrinsic reaction coordinate (IRC)[44,45] calculations were carried out at MP2/6-311G(d,p) level of theory. Single-point energies along the IRC were calculated at CCSD(T)/cc-pVDZ and CCSD(T)/cc-pVTZ levels of theory and extrapolated to the CBS limit.

All quantum chemical calculations were performed with the Gaussian09[46] program package in frozen-core approximation employing the spin-restricted and spin-unrestricted formalism for closed-shell and open-shell species, respectively.[30]

3.2. Rate Coefficients. By assuming equilibrium between the bimolecular reactants and the prereaction complex, the rate coefficient of reaction R1 can be expressed in the form $k_1 = K_{1a}k_{1b}$ with K_{1a} being the equilibrium constant of reaction R1a and k_{1b} being the rate coefficient of reaction R1b.[47] From statistical thermodynamics and canonical transition state theory,[48,49] it follows:

$$k_1(T) = \frac{k_B T}{h} \sum_i \kappa_i(T) L_i \frac{Q_{TS(i)}(T)}{Q_{DME}(T) Q_{OH}(T)} \exp\left(-\frac{\Delta E_{0(i)}}{k_B T}\right) \quad (1)$$

with i = (op, ip) to account for the two different reaction pathways. Here, k_B represents Boltzmann's constant and h denotes Planck's constant. The quantities Q_j represent the partition functions of species j, and $\Delta E_{0(i)}$ is the zero-point-corrected energy difference between TS(i) and the bimolecular reactants, OH + DME/DME-d_6. The partition functions were calculated in rigid rotor/harmonic oscillator approximation, by using wavenumbers scaled with the following factors: 0.9504 (for wavenumbers calculated at MP2/6-311G(d,p) level of theory),[50] 0.947 (CCSD/cc-pVDZ),[51] and 0.99 (B3LYP/6-311G(2d,d,p))[43]. Symmetry numbers in the rotational partition functions are omitted and instead included in the statistical factors L_i;[47,52] one obtains $L_{op} = 4$ and $L_{ip} = 2$.[52] All species were assumed to be in the electronic ground state except OH, for which the electronic partition function was calculated with a spin orbit splitting of 139.7 cm^{-1}.[53]

Tunneling correction factors, $\kappa_i(T)$, were calculated as proposed in ref 54 with the classical potential obtained from the IRC calculations mentioned above and interpolated by a cubic spline function. The method relies on the semiclassical WKB (Wentzel−Kramers−Brillouin) approximation of quantum mechanics.[55−57] We compared these values with results from the Wigner approximation[58,59] and found that the latter approach predicts too high tunneling correction factors. We note, however, that for transition states calculated at the CBS-QB3 level of theory, tunneling was nearly negligible even with the Wigner approximation (see below).

4. RESULTS AND DISCUSSION

4.1. Experiments. The DME + OH reaction was investigated in the temperature range 292−651 K at pressures between 5.9 and 20.9 bar. The initial concentrations ranged from 6.05×10^{15} to 1.40×10^{16} cm^{-3} for HNO_3 and from 1.98×10^{16} to 8.02×10^{16} cm^{-3} for DME. The experiments on the DME-d_6 + OH reaction were carried out in a temperature range of 388 to 554 K at pressures between 13.0 and 20.4 bar with initial concentrations of 1.05×10^{17} to 1.74×10^{17} cm^{-3} for DME-d_6 and 7.79×10^{15} to 1.11×10^{16} cm^{-3} for HNO_3. Under our photolysis conditions, initial concentrations of OH in the order of $\sim 10^{12}$ cm^{-3} arise.[28]

An example for a measured LIF intensity-time profile is shown in Figure 1. From the slopes of the linearized plots,

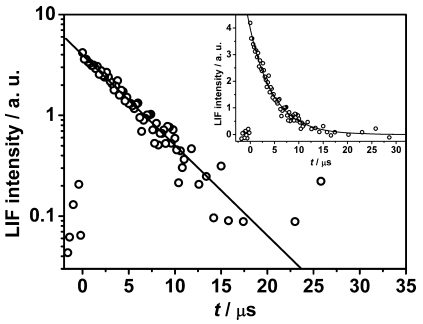

Figure 1. LIF intensity-time profile and least-squares fit for DME + OH at T = 324 K, P = 18.9 bar, and $[DME]_0 = 7.21 \times 10^{16}$ cm^{-3}.

pseudofirst-order rate coefficients, k_{pseudo}, can be obtained, and the second-order rate coefficients, k_1, follow from

$$k_1 = \frac{k_{pseudo,1}}{[DME]_0} = \frac{k_{pseudo} - k_{OH+HNO_3}[HNO_3]_0}{[DME]_0} \quad (2)$$

with an analogous expression for DME-d_6. The rate coefficient of the OH + HNO_3 reaction, $k_{OH+HNO3}$, was determined in separate experiments under similar conditions (T = 293−369 K, P = 4.8−17.6 bar), and we obtained $k_{OH+HNO3} = 1.1 \times 10^{-13} \exp(553\ K/T)$ cm^3 s^{-1}. These results are a factor of 4−7 higher than recently recommended values,[60] but we note that this recommendation is based on experiments performed at pressures ≤1 bar. Even with our larger values, however, the correction term for OH + HNO_3 in eq 2 did never exceed 5% of k_1. The quality of the pseudofirst-order assumption is demonstrated in Figure 2. The positive intercept indicated by the experimental points is a characteristic of this special experimental run. For other runs, we obtained small positive or negative intercepts scattering around zero and, therefore,

dx.doi.org/10.1021/jp405724a | J. Phys. Chem. A 2013, 117, 8343−8351

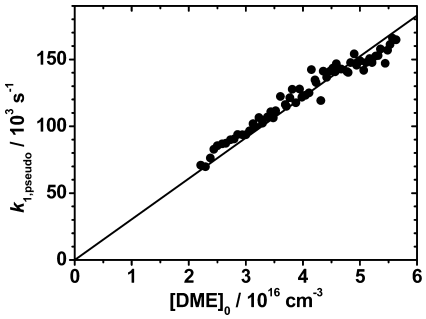

Figure 2. Plot of the pseudofirst-order rate coefficient $k_{1,pseudo}$ vs $[DME]_0$ for T = 325 K and 5.0 ≤ P/bar ≤ 13.5. The linear fit through the origin gives a slope of $k_{1,DME}$ = 3.05 × 10^{12} cm^3 s^{-1}.

decided to generally force our linear fits through the origin. The most likely reason for the differing behavior of different experimental runs are small errors during mixture preparation. The experimental run shown in Figure 2 is the one with the most data points (61), covering the widest range of $[DME]_0$. Usually, a series of 20 measurements were performed at each temperature, and the results were averaged. The rate coefficients k_1 obtained are displayed in Figure 3.

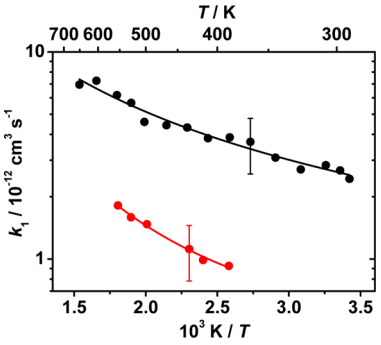

Figure 3. Arrhenius plot of the measured rate coefficients k_1: (black circle) DME + OH; (red circle) DME-d_6 + OH; (solid lines) best fits of eqs 3 and 4, respectively; estimated error ±30%.

The numerical values and the specific experimental conditions are collected in Tables 1S and 2S of the Supporting Information. The following modified Arrhenius expressions were obtained as best fits to the experimental results (see Figure 3):

$$k_{1,DME} = (4.5 \pm 1.4) \times 10^{-16}\left(\frac{T}{K}\right)^{1.48} \exp\left(\frac{66.6\ K}{T}\right)\ cm^3\ s^{-1} \quad (3)$$

and

$$k_{1,DME-d6} = (7.3 \pm 2.2) \times 10^{-23}\left(\frac{T}{K}\right)^{3.57} \exp\left(\frac{759.8\ K}{T}\right)\ cm^3\ s^{-1} \quad (4)$$

This corresponds to an isotope effect of $k_{1,DME}/k_{1,DME\text{-}d6}$ between 3.3 at 554 K and 4.0 at 398 K.

To examine the pressure dependence of the rate coefficient, an extended series of 61 measurements were carried out over a wide range of pressures from 5.0 to 13.5 bar at a temperature of 325 K. The results are shown in Figure 4. The data points correspond to those of Figure 2, and the apparent, slightly

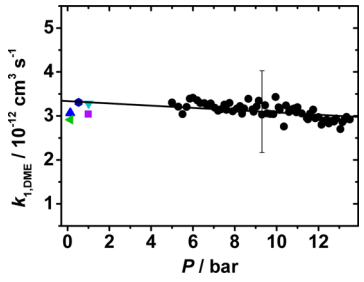

Figure 4. Pressure dependence of the rate coefficient $k_{1,DME}$ at T = 325 K; (black circle) this work with error bar of 30%, (purple square) Arif et al.,[3] (green left facing triangle) Bonard et al.,[4] (light blue downward facing triangle) DeMore and Bayes,[12] (blue upward facing triangle) Mellouki et al.,[5] (navy hexagon) Tully et al.;[7] the average of all values amounts to 3.11 × 10^{-12} cm^3 s^{-1}.

negative pressure dependence is a characteristic of this special experimental run (see above). Other runs gave slightly positive or negative slopes, and we, therefore, consider the pressure dependence to be insignificant, also in view of our estimated maximum error of ±30%.

In Figure 5, our experimental results for the DME + OH reaction are compared with the available data from other

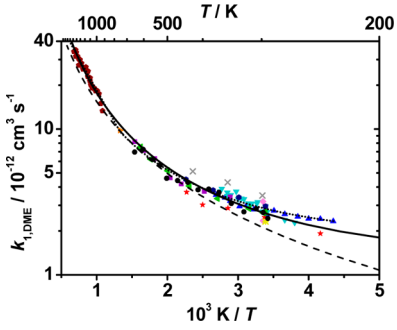

Figure 5. Arrhenius plot of rate coefficients $k_{1,DME}$; (black circle) this work, (purple square) Arif et al.,[3] (green left facing triangle) Bonard et al.,[4] (brown pentagon) Cook et al.,[8] (light blue downward facing triangle) DeMore and Bayes,[12] (blue upward facing triangle) Mellouki et al.,[5] (pink diamond) Nelson et al.,[9] (black ×) Perry et al.,[10] (orange right facing triangle) Tranter and Walker,[13] (navy hexagon) Tully and Droege,[7] (red star) Wallington et al.,[11] (yellow sun) Wallington et al.,[14] (dotted line) fit by Tranter and Walker,[13] (dashed line) estimation by Curran et al.,[62] (solid line) best fit to all experimental values except those from ref 10 (see eq 5).

authors. The agreement is very good. The potential overestimation of the rate coefficient in ref 10, probably a result of impurities, was already discussed in the review of Atkinson.[61] From a fit to all the experimental data points of Figure 5 except the values from ref 10, we obtained the following modified Arrhenius expression, which reproduces the results in the temperature range T = 230−1500 K at pressures between 30 mbar and 21 bar to better than within ±20%:

$$k_{1,DME}(230-1500\ K) = 8.45 \times 10^{-18}\left(\frac{T}{K}\right)^{2.07} \exp\left(\frac{262.2\ K}{T}\right)\ cm^3\ s^{-1} \quad (5)$$

4.2. Quantum Chemical Calculations. A schematic potential energy diagram calculated for the reactions DME + OH and DME-d_6 + OH is displayed in Figure 6. It becomes

dx.doi.org/10.1021/jp405724a | J. Phys. Chem. A 2013, 117, 8343−8351

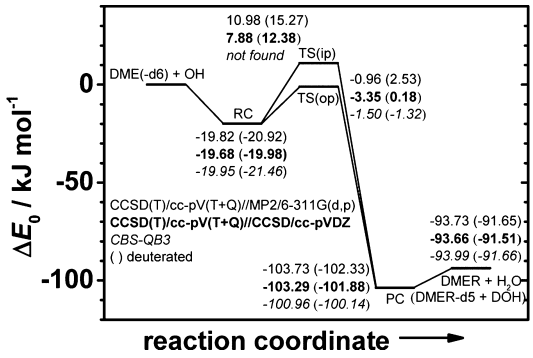

Figure 6. Potential energy diagram (including zero-point energies) for the reactions DME + OH and DME-d_6 + OH; energies are relative to reactant energies.

evident that all three methods applied predict the occurrence of a prereaction and a postreaction complex. Furthermore, two transition states, TS(ip) and TS(op), could be located at CCSD(T)/cc-pV(T,Q)Z//MP2/6-311G(d,p) and CCSD(T)/cc-pV(T,Q)Z//CCSD/cc-pVDZ levels of theory, whereas CBS-QB3 did not predict TS(ip). For all stationary points, the energies calculated with the different methods do not differ by more than 3.1 kJ mol^{-1}. Also, a comparison with recently published[19] results obtained from CCSD(T)/CBS//MP2/6-311G(d,p), G3, and G3MP2BH&H calculations revealed a very good agreement. There are mechanistic differences only regarding the reaction channel via TS(ip). Here, Zhou et al.[19] postulate a direct abstraction reaction, whereas our IRC calculations, as displayed in Figure 7, favor a reaction via the prereaction complex RC also in this case.

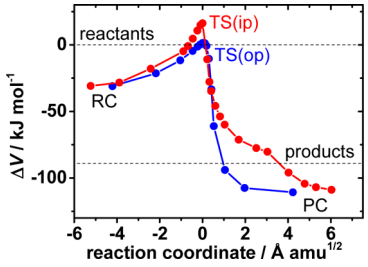

Figure 7. Potential energy (without zero-point energy) vs intrinsic reaction coordinate for the DME + OH reaction calculated at the CCSD(T)/cc-pV(T,Q)Z//MP2/6-311G(d,p) level of theory; (blue) starting from TS(op) and (red) starting from TS(ip); energies are relative to reactant energies.

An unexpected effect was observed in the case of CBS-QB3 calculations. Whereas similar changes of zero-point energy upon deuteration were predicted for each stationary point by the different methods (cf. Figure 6), the situation is different for TS(op). Here, CCSD(T)/cc-pV(T,Q)Z//MP2/6-311G(d,p) and CCSD(T)/cc-pV(T,Q)Z//CCSD/cc-pVDZ gave an increase of 3.49 and 3.53 kJ·mol^{-1}, respectively, whereas CBS-QB3 (with geometry optimization at B3LYP/6-311G(2d,d,p) level of theory) gave only 0.18 kJ·mol^{-1} (cf. Figure 6).

The reason for this behavior are the different geometries of TS(op) obtained with MP2/6-311G(d,p) and CCSD/cc-pVDZ, on the one hand, and with B3LYP/6-311G(2d,d,p), on the other hand. The most important features are summarized in Figure 8, and the complete information on the geometries is given in the Supporting Information.

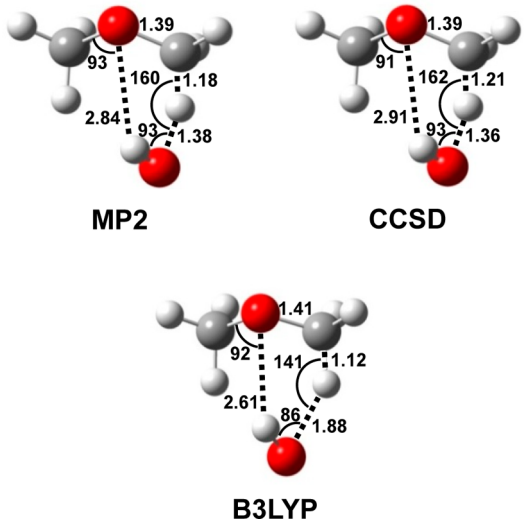

Figure 8. Geometries of TS(op) calculated with MP2/6-311G(d,p), CCSD/cc-pVDZ, and B3LYP/6-311G(2d,d,p), respectively (bond lengths in 10^{-10} m; bond angles in degrees).

For MP2 and CCSD, the hydrogen bond between ether oxygen and hydroxyl hydrogen is strongly expanded in going from RC to TS(op) (from 1.87 × 10^{-10} to 2.84 × 10^{-10} and from 1.89 × 10^{-10} to 2.91 × 10^{-10} m, respectively), and the O···H···C configuration in TS(op) is almost collinear (160 and 162°, respectively). The forming O−H bond has a bond length of 1.38 × 10^{-10} and 1.36 × 10^{-10} m, respectively, and the breaking C−H bond is only a little shorter, namely, 1.18 × 10^{-10} and 1.21 × 10^{-10} m, respectively. Accordingly, the reaction coordinate most closely corresponds to a translational motion of the migrating *hydrogen* atom (as one would expect). The imaginary wavenumbers are 1482i and 1354i cm^{-1}, respectively.

In contrast, for B3LYP the hydrogen bond between ether oxygen and hydroxyl hydrogen is somewhat less expanded (from 1.85 × 10^{-10} to 2.61 × 10^{-10} m), and the O···H···C configuration is clearly bent (141°). The forming O−H bond (1.88 × 10^{-10} m) is still much longer than the breaking C−H bond (1.12 × 10^{-10} m), and it turns out that the reaction coordinate more closely corresponds to a torsional motion of the *oxygen* atom O′ within the C−O···H···O′ moiety. This is also reflected in the imaginary wavenumber, which is 158i cm^{-1}, that is, much lower than in the above cases. Accordingly, the curvature of the potential energy surface along the reaction coordinate is much smaller, and the tunneling contribution turns out negligible even in the Wigner approximation (see above).

As a result, the kinetic isotope effect upon H−D substitution that is predicted on the basis of the CBS-QB3 data (reaction coordinate: O atom movement) is much smaller than the isotope effect predicted on the basis of the MP2 and CCSD data (H atom movement). This is a combined effect of differences in zero-point energies and tunneling contributions. A comparison with our experimental results is given below.

From our quantum chemical calculations, also heats of formation for DME and DMER were obtained by using atomization schemes. The results are collected and compared with literature data in Table 1.

4.3. Rate Coefficients. From the results of our quantum chemical calculations, we calculated rate coefficients of reaction

dx.doi.org/10.1021/jp405724a | J. Phys. Chem. A 2013, 117, 8343−8351

Table 1. Heats of Formation Calculated in This Work in Comparison with Values from the Literature

species	$\Delta_f H$ (298.15 K) (kJ mol^{-1})	ref
DME	−182.28	this work[a]
	−182.43	this work[b]
	−188.68	this work[c]
	−184	ref 63
	−184.05	ref 64
	−184.1 ± 0.5	ref 65
DME-d_6	−207.93	this work[a]
	−209.75	this work[b]
	−215.24	this work[c]
DMER	5.47	this work[a]
	5.29	this work[b]
	−0.72	this work[c]
	3.8	ref 63
	−0.10	ref 64
	3.8	refs 65 and 66
	0.17 ± 0.84	ref 19
DMER-d_5	−14.52	this work[a]
	−13.94	this work[b]
	−21.26	this work[c]

[a]CCSD(T)/cc-VD(T+Q)Z//MP2/6-311G(d,p). [b]CCSD(T)/cc-pV-(T,Q)Z//CCSD/cc-pVDZ. [c]CBS-QB3.

R1, using eq 1. The results are displayed and compared with our experimental data in Figure 9. Compact numerical expressions for the calculated temperature dependences are given in the Supporting Information.

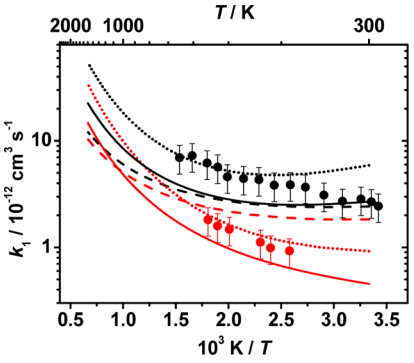

Figure 9. Arrhenius plots of the rate coefficients; (black) DME + OH; (red) DME-d_6 + OH; (solid lines) calculated, CCSD(T)/cc-pV(T,Q)Z//MP2/6-311G(d,p); (dotted lines) calculated, CCSD-(T)/cc-pV(T,Q)Z//CCSD/cc-pVDZ; (dashed lines) calculated, CBS-QB3; (symbols) experimental values.

From Figure 9 it becomes obvious that the rate coefficients calculated from the data obtained at CCSD(T)/cc-pV(T,Q)Z //MP2/6-311G(d,p) and CCSD(T)/cc-pV(T,Q)Z//CCSD/cc-pVDZ level of theory show a very good agreement with the results of our experiments. The absolute values, the temperature dependence, and also the isotope effect are reasonably well described. We note that no adjustments of molecular and energy data were made.

The results based on CBS-QB3 show in general a less good but still acceptable agreement, where the isotope effect is underestimated as was already discussed in section 4.2. Numerical values for the isotope effect are collected in Table 2.

Table 2. Calculated and Measured Isotope Effect of k_1 for Different Temperatures

	$k_{1,DME}/k_{1,DME\text{-}d6}$			
method	400 K	450 K	500 K	550 K
CCSD(T)/cc-pV(T,Q)Z //MP2/6-311G(d,p)	3.8	3.2	2.9	2.6
CCSD(T)/cc-pV(T,Q)Z //CCSD/cc-pVDZ	4.1	3.6	3.2	2.9
CBS-QB3	1.3	1.3	1.2	1.2
experiment	3.9	3.7	3.5	3.2

In Table 3, branching ratios k_1(ip)/k_1(op) are collected. These values were calculated from eq 1 with tunneling

Table 3. Calculated Branching Ratios k_1(ip)/k_1(op) for Different Temperatures and Isotopic Substitution

quantum chemical method	CCSD(T)/cc-pV(T+Q)Z //CCSD/cc-pVDZ		CCSD(T)/cc-pV(T+Q)Z //MP2/6-311G(d,p)	
T (K)	undeuterated	deuterated	undeuterated	deuterated
300	0.13	0.06	0.02	0.01
500	0.52	0.39	0.10	0.07
700	1.09	0.91	0.21	0.17

corrections after ref 54. The corresponding tunneling correction factors, $\kappa_i(T)$, are given in Table 4. From Table 3, it is obvious that at lower temperatures the pathway via the lower lying TS(op) is predominant, but as one would expect, the pathway via the higher lying TS(ip) gains importance as the temperature increases. Deuteration, however, leads to a smaller share via TS(ip) because tunneling is more important for this channel, which is obvious from Table 4. It becomes also evident that tunneling through TS(ip) at 300 K is important even for the deuterated case (tunneling factor κ_{ip}(300 K) = 2.13), but as k_1(ip)/k_1(op) = 0.01, it is less important for the overall reaction (κ_{op}(300 K) = 1.20).

Table 4. Tunneling Correction Factors $\kappa_i(T)$ Calculated from IRC Analysis at CCSD(T)/cc-pV(T,Q)Z//MP2/6-311G(d,p) Level of Theory (cf. Figure 7) for Different Temperatures and Isotopic Substitution

	undeuterated		deuterated	
T (K)	$\kappa_{ip}(T)$	$\kappa_{op}(T)$	$\kappa_{ip}(T)$	$\kappa_{op}(T)$
300	3.84	1.44	2.13	1.20
500	1.63	1.14	1.31	1.07
700	1.28	1.07	1.15	1.03

A most interesting feature, which can be realized from Figure 5, is the missing pressure dependence of the experimental rate coefficient k_1 over a pressure range from 21 bar down to 30 mbar. The reasons for this behavior are difficult to assess. Whereas the pre-equilibrium assumption can be expected to apply at the high pressures of the present work, it is less likely to hold at pressures near 1 bar (where most of the experiments were conducted) or at even lower pressures down to 30 mbar. A master equation calculation performed in ref 19 yields rate coefficients in good agreement with the experimental data, but the pressure for which the calculations were performed is unfortunately not given in the publication. Accordingly, the question as to whether the missing pressure dependence is, e.g., due to an accidental similarity of the low- and high-pressure

dx.doi.org/10.1021/jp405724a | J. Phys. Chem. A 2013, 117, 8343−8351

limiting rate coefficients, to peculiarities of the steady-state regime,[67] or to the applicability of the pre-equilibrium assumption also at lower pressures has to remain an open question. Here, a new master equation modeling, which takes into account the high-pressure rate coefficients of the present work, would provide additional evidence.

5. CONCLUSIONS

The kinetics of the DME + OH reaction was experimentally and theoretically studied. Rate coefficients were determined in the temperature range 292−650 K at pressures between 5.9 and 20.9 bar. The temperature dependence of the rate coefficients was parametrized; a pressure dependence was not observed. The reaction of the isotopologue, DME-d_6 + OH, was also studied. The experiments were supplemented by quantum chemical and statistical rate theory calculations. From the combined results, it follows that the DME + OH reaction proceeds via a prereaction complex, two transition states, and a postreaction complex to give DMER + H_2O. The kinetics can be reasonably well described by canonical transition state theory, with the assumption of an equilibrium between the reactants and the prereaction complex. The rate coefficients and the isotope effect are well predicted on the basis of quantum chemical data obtained at CCSD(T)/cc-pV(T,Q)Z//MP2/6-311G(d,p) and CCSD(T)/cc-pV(T,Q)Z//CCSD/cc-pVDZ level of theory, whereas density functional theory at B3LYP/6-311G(2d,d,p) level probably predicts wrong geometries of the transitions states. The existence of a prereaction complex is a clear indication for the importance of long-range interactions in a reactive system. The use of DFT for locating transition states should be avoided when contributions from π stacking and/or hydrogen bonding interactions are expected to be high. In these cases, at least the DFT results must be checked against CCSD results to assess the reliability of the transition state structures obtained. An explanation of the missing pressure dependence of the rate coefficient experimentally observed also at lower pressures calls for a detailed master equation analysis, which is, however, beyond the scope of the present work.

■ ASSOCIATED CONTENT

Supporting Information

Experimental conditions and measured rate coefficients, optimized geometries, calculated wavenumbers and rotational constants, and modified Arrhenius expressions for calculated rate coefficients. This material is available free of charge via the Internet at http://pubs.acs.org.

■ AUTHOR INFORMATION

Corresponding Author

*(M.O.) E-mail: matthias.olzmann@kit.edu.

Present Address

[†]Department of Chemical Informatics, Faculty of Education, University of Szeged, Boldogasszony sgt. 6, Szeged 6725, Hungary.

Notes

The authors declare no competing financial interest.

■ ACKNOWLEDGMENTS

Support of this work from the Deutsche Forschungsgemeinschaft (FOR 1447, "Physicochemical-Based Models for the Prediction of Safety-Relevant Ignition Processes") is gratefully acknowledged. We wish to thank Bettina Derstroff for help with the experiments on the OH + HNO_3 reaction. One of the authors (M.S.) is thankful for support within TÁMOP-4.2.2.A-11/1/KONV-2012-0047, "New Functional Materials and Their Biological and Environmental Answers", and TÁMOP 4.2.4.A/2-11-1-2012-0001, "National Excellence Program: Elaborating and Operating an Inland Student and Researcher Personal Support System", subsidized by the European Union and cofinanced by the European Social Fund (A2-MZPD-12-0139).

■ REFERENCES

(1) Kohse-Höinghaus, K.; Oßwald, P.; Cool, T. A.; Kasper, T.; Hansen, N.; Qi, F.; Westbrook, C. K.; Westmoreland, P. R. Biofuel Combustion Chemistry: From Ethanol to Biodiesel. *Angew. Chem., Int. Ed.* **2010**, *49*, 3572−3597.

(2) Arcoumanis, C.; Bae, C.; Crookes, R.; Kinoshita, E. The Potential of Dimethyl Ether (DME) as an Alternative Fuel for Compression-Ignition Energies. *Fuel* **2008**, *87*, 1014−1030.

(3) Arif, M.; Dellinger, B.; Taylor, P. H. Rate Coefficients of Hydroxyl Radical Reaction with Dimethyl Ether and Methyl *tert*-Butyl Ether over an Extended Temperature Range. *J. Phys. Chem. A* **1997**, *101*, 2436−2441.

(4) Bonard, A.; Daëlle, V.; Delfau, J.-L.; Vovelle, C. Kinetics of OH Radical Reactions with Methane in the Temperature Range 295−660 K and with Dimethyl Ether and Methyl-*tert*-butyl Ether in the Temperature Range 295−618 K. *J. Phys. Chem. A* **2002**, *106*, 4384−4389.

(5) Mellouki, A.; Teton, S.; Le Bras, G. Kinetics of OH Radical Reactions with a Series of Ethers. *Int. J. Chem. Kinet.* **1995**, *27*, 791−805.

(6) Shannon, R. J.; Taylor, S.; Goddard, A.; Blitz, M. A.; Heard, D. E. Observation of a Large Negative Temperature Dependence for Rate Coefficients of Reactions of OH with Oxygenated Volatile Organic Compounds Studied at 86−112 K. *Phys. Chem. Chem. Phys.* **2010**, *12*, 13511−13514.

(7) Tully, F. P.; Droege, A. T. Kinetics of the Reactions of the Hydroxyl Radical with Dimethyl Ether and Diethyl Ether. *Int. J. Chem. Kinet.* **1987**, *19*, 251−259.

(8) Cook, R. D.; Davidson, D. F.; Hanson, R. K. High-Temperature Shock Tube Measurements of Dimethyl Ether Decomposition and the Reaction of Dimethyl Ether with OH. *J. Phys. Chem. A* **2009**, *113*, 9974−9980.

(9) Nelson, L.; Rattigan, O.; Neavyn, R.; Sidebottom, H.; Treacy, J.; Nielsen, O. J. Absolute and Relative Rate Constants for the Reactions of Hydroxyl Radicals and Chlorine Atoms with a Series of Aliphatic Alcohols and Ethers at 298 K. *Int. J. Chem. Kinet.* **1990**, *22*, 1111−1126.

(10) Perry, P. A.; Atkinson, R.; Pitts, J. N. Rate Constants for the Reaction of OH Radicals with Dimethyl Ether and Vinyl Ether over the Temperature Range 299−427 K. *J. Chem. Phys.* **1977**, *67*, 611−614.

(11) Wallington, T. J.; Liu, R.; Dagaut, P.; Kurylo, M. J. The Gas Phase Reactions of Hydroxyl Radicals with a Series of Aliphatic Ethers over the Temperature Range 240−440 K. *Int. J. Chem. Kinet.* **1988**, *20*, 41−49.

(12) DeMore, W. B.; Bayes, K. D Rate Constants for the Reaction of Hydroxyl Radical with Several Alkanes, Cycloalkanes and Dimethyl Ether. *J. Phys. Chem. A.* **1999**, *103*, 2649−2654.

(13) Tranter, R. S.; Walker, R. W. Rate Constants for the Reactions of H Atoms and OH Radicals with Ethers at 753 K. *Phys. Chem. Chem. Phys.* **2001**, *3*, 4722−4732.

(14) Wallington, T. J.; Andino, J. M.; Skewes, L. M.; Siegl, W. O.; Japar, S. M. Kinetics of the Reaction of OH Radicals with a Series of Ethers under Simulated Atmospheric Conditions at 295 K. *Int. J. Chem. Kinet.* **1989**, *21*, 993−1001.

(15) Atandinç, F.; Selçuki, C.; Sari, L.; Aviyente, V. Theoretical Study of Hydrogen Abstraction from Dimethyl Ether and Methyl *tert*-Butyl

Ether by Hydroxyl Radical. *Phys. Chem. Chem. Phys.* **2002**, *4*, 1797−1806.
(16) Bottoni, A.; Della Casa, P.; Poggi, G. Reactions between the OH Radical and Oxygen-Containing Atmospheric Pollutants: a Theoretical Description. *J. Mol. Struct. (THEOCHEM)* **2001**, *542*, 123−137.
(17) El-Nahas, A. M.; Uchimaru, T.; Sugie, M.; Tokuhashi, K.; Sekiya, A. Hydrogen Abstraction from Dimethyl Ether (DME) and Dimethyl Sulfide (DMS) by OH Radical: a Computational Study. *J. Mol. Struct. (THEOCHEM)* **2005**, *722*, 9−19.
(18) Zavala-Oseguera, C.; Alvaraz-Idaboy, J. R.; Merino, G.; Galano, A. OH Radical Gas Phase Reactions with Aliphatic Ethers: A Variational Transition State Theory Study. *J. Phys. Chem. A.* **2009**, *113*, 13913−13920.
(19) Zhou, C.-W.; Simmie, J. M.; Curran, H. J. An ab Initio/Rice-Ramsperger-Kassel-Marcus Study of the Hydrogen-Abstraction Reactions of Methyl Ethers, H_3COCH_3-$x(CH_3)_x$, x = 0−2, by OH; Mechanism and Kinetics. *Phys. Chem. Chem. Phys.* **2010**, *12*, 7221−7233.
(20) Wu, J.-Y.; Liu, J.-Y.; Li, Z.-S.; Sun, C.-C. Dual-Level Direct Dynamics Studies for the Reactions of CH_3OCH_3 and CF_3OCH_3 with the OH Radical. *J. Chem. Phys.* **2003**, *118*, 10986−10995.
(21) Ogura, T.; Miyoshi, A.; Koshi, M. Rate Coefficients of H-Atom Abstraction from Ethers and Isomerization of Alkoxyalkylperoxy Radicals. *Phys. Chem. Chem. Phys.* **2007**, *9*, 5133−5142.
(22) Černý, J.; Hobza, P. Non-Covalent Interactions in Biomacromolecules. *Phys. Chem. Chem. Phys.* **2007**, *9*, 5291−5303.
(23) Johnston, H. S. *Gas Phase Reaction Rate Theory*; Ronald: New York, 1966.
(24) Forster, R.; Frost, M.; Fulle, D.; Hamann, H. F.; Hippler, H. High Pressure Range of the Addition of HO to HO, NO, NO2, and CO. I. Saturated Laser Induced Fluorescence Measurements at 298 K. *J. Chem. Phys.* **1995**, *103*, 2949−2958.
(25) Hippler, H.; Striebel, F.; Viskolcz, B. A Detailed Experimental and Theoretical Study on the Decomposition of Methoxy Radicals. *Phys. Chem. Chem. Phys.* **2001**, *3*, 2450−2458.
(26) Welz, O.; Striebel, F.; Olzmann, M. On the Thermal Unimolecular Decomposition of the Cyclohexoxy Radical: An Experimental and Theoretical Study. *Phys. Chem. Chem. Phys.* **2008**, *10*, 320−329.
(27) Welz, O.; Olzmann, M. Kinetics of the NCN + NO Reaction over a Broad Temperature and Pressure Range. *J. Phys. Chem. A* **2012**, *116*, 7293−7301.
(28) Kappler, C.; Zádor, J.; Welz, O.; Fernandes, R. X.; Olzmann, M.; Taatjes, C. A. Competing Channels in the Propene + OH Reaction: Experiment and Validated Modeling over a Broad Temperature and Pressure Range. *Z. Phys. Chem.* **2011**, *225*, 1271−1291.
(29) Møller, C.; Plesset, M. S. Note on an Approximation Treatment for Many-Electron Systems. *Phys. Rev.* **1934**, *46*, 618−622.
(30) Hehre, W. J.; Radom, L.; Schleyer, P. v. R.; Pople, J. A. *Ab Initio Molecular Orbital Theory*; Wiley: New York, 1986.
(31) Krishnan, R.; Frisch, M. J.; Pople, J. A. Contribution of Triple Substitutions to the Electron Correlation Energy in Fourth Order Perturbation Theory. *J. Chem. Phys.* **1980**, *72*, 4244−4245.
(32) Čížek, J. On the Correlation Problem in Atomic and Molecular Systems. Calculation of Wavefunction Components in Ursell-Type Expansion Using Quantum-Field Theoretical Methods. *J. Chem. Phys.* **1966**, *45*, 4256−4266.
(33) Purvis, J. D., III; Bartlett, R. J. A Full Coupled-Cluster Singles and Doubles Model: The Inclusion of Disconnected Triples. *J. Chem. Phys.* **1982**, *76*, 1910−1918.
(34) Dunning, T. H., Jr. Gaussian Basis Sets for Use in Correlated Molecular Calculations. I. The Atoms Boron through Neon and Hydrogen. *J. Chem. Phys.* **1989**, *90*, 1007−1023.
(35) Kendall, R. A.; Dunning, T. H., Jr.; Harrison, R. J. Electron Affinities of the First-Row Atoms Revisited. Systematic Basis Sets and Wave Functions. *J. Chem. Phys.* **1992**, *96*, 6796−6806.
(36) Pople, J. A.; Head-Gordon, M.; Raghavachari, K. Quadratic Configuration Interaction. A General Technique for Determining Electron Correlation Energies. *J. Chem. Phys.* **1987**, *87*, 5968−5975.
(37) Feller, D. The Use of Systematic Sequences of Wave Functions for Estimating the Complete Basis Set, Full Configuration Interaction Limit in Water. *J. Chem. Phys.* **1993**, *98*, 7059−7071.
(38) Helgaker, T.; Klopper, W.; Koch, H.; Noga, J. Basis-Set Convergence of Correlated Calculations on Water. *J. Chem. Phys.* **1997**, *106*, 9639−9646.
(39) Lee, T. J.; Taylor, P. R. A Diagnostic for Determining the Quality of Single-Reference Electron Correlation Methods. *Int. J. Quant. Chem. Symp.* **1989**, *23*, 199−207.
(40) Parr, R. G.; Yang, W. *Density-Functional Theory of Atoms and Molecules*; Oxford University Press: Oxford, U.K., 1989.
(41) Becke, A. D. Density-Functional Thermochemistry. III. The Role of Exact Exchange. *J. Chem. Phys.* **1993**, *98*, 5648−5652.
(42) Stephens, P. J.; Devlin, F. J.; Chabalowski, C. F.; Frisch, M. J. Ab Initio Calculation of Vibrational Absorption and Circular Dichroism Spectra Using Density Functional Force Fields. *J. Phys. Chem.* **1994**, *98*, 11623−11627.
(43) Montgomery, J. A., Jr.; Frisch, M. J.; Ochterski, J. W.; Petersson, G. A. A Complete Basis Set Model Chemistry. VI. Use Of Density Functional Geometries and Frequencies. *J. Chem. Phys.* **1999**, *110*, 2822−2827.
(44) Gonzalez, C.; Schlegel, H. B. An Improved Algorithm for Reaction Path Following. *J. Chem. Phys.* **1989**, *90*, 2154−2161.
(45) Gonzalez, C.; Schlegel, H. B. Reaction Path Following in Mass-Weighted Internal Coordinates. *J. Phys. Chem.* **1990**, *94*, 5523−5527.
(46) Frisch, M. J.; Trucks, G. W.; Schlegel, H. B.; Scuseria, G. E.; Robb, M. A.; Cheeseman, J. R.; Scalmani, G.; Barone, V.; Mennucci, B.; Petersson, G. A.; et al. *Gaussian 09*, revision A.1; Gaussian, Inc.: Wallingford, CT, 2009.
(47) Steinfeld, J. I.; Francisco, J. S.; Hase, W. L. *Chemical Kinetics and Dynamics*; Prentice Hall: Englewood Cliffs, NJ, 1989.
(48) Hill, T. L. *An Introduction to Statistical Thermodynamics*; Addison-Wesley: Reading, MA, 1960.
(49) Glasstone, S.; Laidler, K. J.; Eyring, H. *The Theory of Rate Processes*; McGraw-Hill: New York, 1941.
(50) Merrick, J. P.; Moran, D.; Radom, L. An Evaluation of Harmonic Vibrational Frequency Scale Factors. *J. Phys. Chem. A* **2007**, *111*, 11683−11700.
(51) Russell D. Johnson III., Ed. NIST Computational Chemistry Comparison and Benchmark Database, NIST Standard Reference Database Number 101 Release 15b, August 2011; see http://cccbdb.nist.gov/.
(52) Gilbert, R. G.; Smith, S. C. *Theory of Unimolecular and Recombination Reactions*; Blackwell: Oxford, U.K., 1990.
(53) Herzberg, G. *Molecular Spectra and Molecular Structure, Vol. I: Spectra of Diatomic Molecules*; 2nd ed.; Krieger: Malabar, FL, 1989.
(54) Garrett, B. C.; Truhlar, D. G. Semiclassical Tunneling Calculations. *J. Phys. Chem.* **1979**, *83*, 2921−2926.
(55) Wentzel, G. Eine Verallgemeinerung der Quantenbedingung für die Zwecke der Wellenmechanik. *Z. Phys.* **1926**, *38*, 518−529.
(56) Kramers, H. A. Wellenmechanik und halbzahlige Quantisierung. *Z. Phys.* **1926**, *39*, 828−840.
(57) Brillouin, L. Remarques sur la mécanique ondulatoire. *J. Phys. Radium* **1926**, *7*, 353−368.
(58) Wigner, E. Über das Überschreiten von Potentialschwellen bei Chemischen Reaktionen. *Z. Phys. Chem.* **1932**, *B19*, 203−216.
(59) Henriksen, N. E.; Hansen, F. Y. *Theories of Molecular Reaction Dynamics*; Oxford University Press: Oxford, U.K., 2008.
(60) Atkinson, R.; Baulch, D. L.; Cox, R. A.; Crowley, J. N.; Hampson, R. F.; Hynes, R. G.; Jenkin, M. E.; Rossi, M. J.; Troe, J. Evaluated Kinetic and Photochemical Data for Atmospheric Chemistry: Volume I, Gas Phase Reactions of O_x, HO_x, NO_x and SO_x Species. *Atmos. Chem. Phys.* **2004**, *4*, 1461−1738.
(61) Atkinson, R. Kinetics and Mechanisms of the Gas-Phase Reactions of the Hydroxyl Radical with Organic Compounds under Atmospheric Conditions. *Chem. Rev.* **1985**, *85*, 69−201.
(62) Curran, H. J.; Pitz, W. J.; Westbrook, C. K.; Dagaut, P.; Boettner, J.-C.; Cathonnet, M. A Wide Range Modeling Study of Dimethyl Ether Oxidation. *Int. J. Chem. Kinet.* **1998**, *30*, 229−241.

(63) Good, D. A.; Francisco, J. S. Heat of Formation of CH_3OCH_2 Radical. *Chem. Phys. Lett.* **1997**, *266*, 512−514.
(64) Baulch, D. L.; Bowman, C. T.; Cobos, C. J.; Cox, R. A.; Just, T.; Kerr, J. A.; Pilling, M. J.; Stocker, D.; Troe, J.; Tsang, W.; Walker, R. W.; Warnatz, J. Evaluated Kinetic Data for Combustion Modeling: Supplement II. *J. Phys. Chem. Ref. Data* **2005**, *34*, 757−1397.
(65) Sander, S. P.; Abbatt, J.; Barker, J. R.; Burkholder, J. B.; Friedl, R. R.; Golden, D. M.; Huie, R. E.; Kolb, C. E.; Kurylo, M. J.; Moortgat, G. K.; Orkin, V. L.; Wine, P. H. *Chemical Kinetics and Photochemical Data for Use in Atmospheric Studies*, Evaluation No. 17, JPL Publication 10-6; Jet Propulsion Laboratory: Pasadena, CA, 2011; see http://jpldataeval.jpl.nasa.gov.
(66) Sumathi, R.; Green, W. L., Jr. Oxygenate, Oxyalkyl and Alkoxycarbonyl Thermochemistry and Rates for Hydrogen Abstraction from Oxygenates. *Phys. Chem. Chem. Phys.* **2003**, *5*, 3402−3417.
(67) Olzmann, M. In *Cleaner Combustion: Developing Detailed Chemical Kinetic Models*; Battin-Leclerc, F., Simmie, J. M., Blurock, E., Ed.; Springer: London, U.K., 2013; Chapter 21.